

## Electronic Supplementary Information (ESI)

# Thin-Film-Transistor Digital Microfluidics for High Value in Vitro Diagnostics at the Point-of-Need

Sally Anderson, Ben Hadwen, Chris Brown

### Contents

**S1: TFT backplane**

**S2: Droplet manipulation algorithms**

**S3: Microfluidic Cartridge**

**S4: Control Instrumentation**

**S5: Illumina Next Generation Sequencing: DNA Library Preparation Protocols on aQdrop™**

**S6: Protocol Development on aQdrop for IVD at the Point of Need**

**S7: Description of Supporting Videos**

**S8: References**

### **S1: TFT backplane – pixel circuit operation and self-test mode**

The TFT backplane of the device is an active matrix array of 316 x 130 elements. Each element has an associated electrode of size 207 μm x 207 μm and adjacent electrodes are separated by a gap of 3 μm. The electrodes are formed from Indium Zinc Oxide (IZO) and are arranged atop the TFT control circuitry for controlling the element. Each array element circuit performs the dual functions of providing an electro-wetting actuation voltage to the electrode and sensing the capacitance presented at each electrode to determine the size and positions of the droplets. The design and operation of the pixel circuit is explained with reference to Fig. S1.1 below. Table S1.1 summarises high-level specification and performance of the chip. A number of additional features have been implemented in the integrated row and column drivers compared to the previously reported state of the art. Firstly, high frame rates for data writing and sensing, similar to [3] but on an array with approximately x2.5 the total number of elements, are achieved by multiplexing the digital data input (x4) and analogue sensor output (x2). The digital control electronics also provides a mode whereby data can be selectively written or sensed to a subset of rows in the array within each frame, in accordance with the location of the droplets and the change in actuation pattern. Therefore, droplet motion with speeds of 50 elements / second and above could be achieved whilst still employing closed loop sensor feedback, maximum droplet speed being limited only by the physical droplet properties and not the addressing electronics. Secondly, the control electronics has a variant mode of operation whereby the content of data written can be read-out through the sensor. This creates a “self-test” mode of operation allowing the functionality of each element to be individually tested. A software application to systematically scan the array and verify correct operation was created and can be executed in 3 seconds. The “self-test” is thus performed as an outgoing inspection in manufacture as well as immediately before and immediately after the execution of the droplet protocol and verifies the correct operation of the device. The TFT backplane was fabricated by Sharp Corporation on a glass substrate (AN100, 0.5mm thickness, Asahi glass) using their “Advanced CG Silicon™” process, which is identical to that used for LCD smartphone display manufacture up to and including the electrode layer. The uppermost layer of the process is a 300nm silicon nitride deposited by PECVD and forms the ion barrier insulator layer of the EWOD construction.

### **Electro-wetting actuation**

The array element contains an SRAM memory element, the programmed state of which determines whether electro-wetting actuation is turned on or off. The data content input through a x4 MUX serial interface, and data is written row at a time by loading +10V or -10V onto the column line DATA and taking gate line GL high briefly to open switch T2 and close switch T1 writing data to the SRAM. An AC voltage actuation signal is passed through to the electrode of each array element, which is either one of global signals ACT or ACTB according to whether the SRAM is programmed “1” or “0”. The same ACTB signal is also supplied to the top plate electrode, so that if the array element is programmed “1”, the potential difference between the electrode and the top plate electrode is an AC voltage waveform of twice the amplitude of ACT. An AC signal is found to be necessary to avoid voltage shift and reliability problems due to the trapping of charge in dielectric insulator layers.

## Capacitance sensor

The capacitance sensor function operated by comparing the load impedance at the electrode with a reference capacitance  $C_1$ . Except when a row is being sensed, reset signal RST is maintained high, so that transistor T4 is on and the potential at the gate of T3 is maintained at a low level, with T3 turned off. The sensor is operated row at a time, with timings as shown in Fig. S1.1c. Firstly RST is taken low to turn T4, then SEL is taken low to turn off T5 and briefly disconnect the electrode from the actuation signal, and then a voltage pulse of amplitude  $\Delta V = 10V$  is supplied to signal RWS. This is coupled through to the electrode, with an amplitude that depends on the ratio of  $C_1$  to the load capacitance at the electrode. The perturbation is further coupled across  $C_2$  to the gate of T3, whereupon T3 is turned on to an extent that depends on the capacitance at the electrode, the potential at this node becoming:

$$V = V_{RST} + \Delta V \frac{C_2}{C_2 + C_L + C_{par1}} \times \frac{C_C}{C_C + C_{par2}}$$

Where  $V_{RST}$  is the reset potential,  $C_{par1}$  is the parasitic capacitance at the electrode,  $C_{par2}$  is the parasitic capacitance at the gate of T3 and  $C_L$  the capacitance at the electrode represented by the load.

The sensor column amplifier (not in the array element), measures the total current sunk through T3 during the time period of RWS, converts this signal to a voltage and serialises it, for readout at up to 1MHz through one of two sensor output amplifiers.

## Self-test mode of operation

Self-test mode of operation is configured with a variant set of timings, shown in Fig. S1.1d. The SRAM memory element is programmed and a perturbation voltage input through ACT. SEL remains high, T5 remains turned on, and the perturbation of coupled through to the sensor circuit. In the event of each array element functioning correctly, the sensor “image” readout thus matches the “image” of data programmed, verifying the correct operation of the circuitry. The self-test mode is also implemented in an inverted mode with the array element programmed “0” and the signal from ACTB passed through to the sensor. Therefore, every transistor in the array is verified.

<b>Chip specifications</b>		<b>Value</b>	<b>Units</b>
Glass dimensions		78 x 34	mm
Electro-wetting array dimensions		27.3 x 66.36	mm
Array format		316 x 130	
Electrode size		207 x 207	µm
Electrode gap		3	
Number of terminal connector pins		48	
<b>Actuation and data write</b>			
Actuation signal input frequency (serial data, each of x4 channels)		1	MHz
Whole data frame write time (typical timings)		16.91	ms
Maximum electro-wetting actuation voltage		20	Volts
Rows can be written selectively		Yes	
<b>Capacitance Sensor operation</b>			
Sensor signal output frequency (serial analogue signal, each of x2 outputs)		1	MHz
Sensor frame measurement time (typical timings)		36.24	ms
Rows can be sensed selectively		Yes	
<b>Capacitance Sensor characterisation data</b>			
<b>Sensor signal characteristics</b>			
Sensor output voltage	No droplet	7.2	Volts
	Droplet	3.8	Volts
	Signal swing	3.4	Volts
<b>Interaction of actuation function with sensor</b>			
Change in sensor output voltage due to actuation	Droplet	<5	mV
	No droplet	<5	mV
<b>Sensor Noise</b>			
Row fixed pattern noise	Droplet	16	mV
	No droplet	18	mV
Column Fixed Pattern noise	Droplet	66	mV
	No droplet	53	mV
Pixel Fixed Pattern Noise	Droplet	108	mV
	No droplet	181	mV
Total Fixed Pattern Noise	Droplet	121	mV
	No droplet	194	mV
Signal to Fixed Pattern Noise ratio	Droplet	28.1	-
	No droplet	17.5	-
Transient noise		<3	mV

Table S1.1. TFT backplane specifications and electrical performance parameters

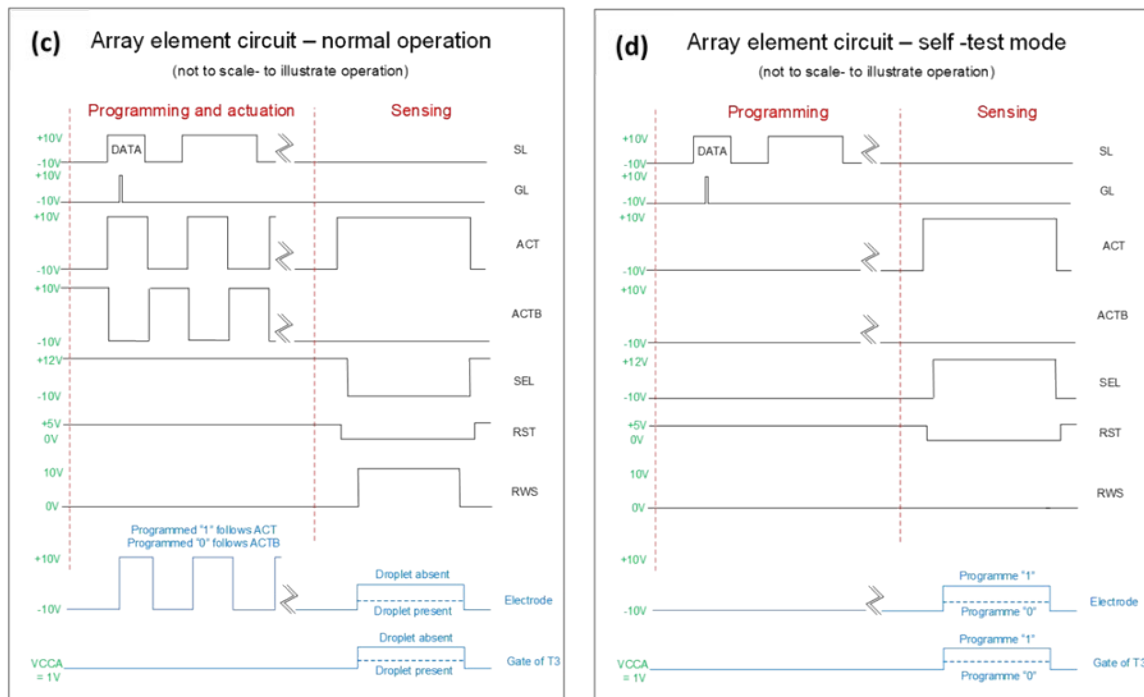
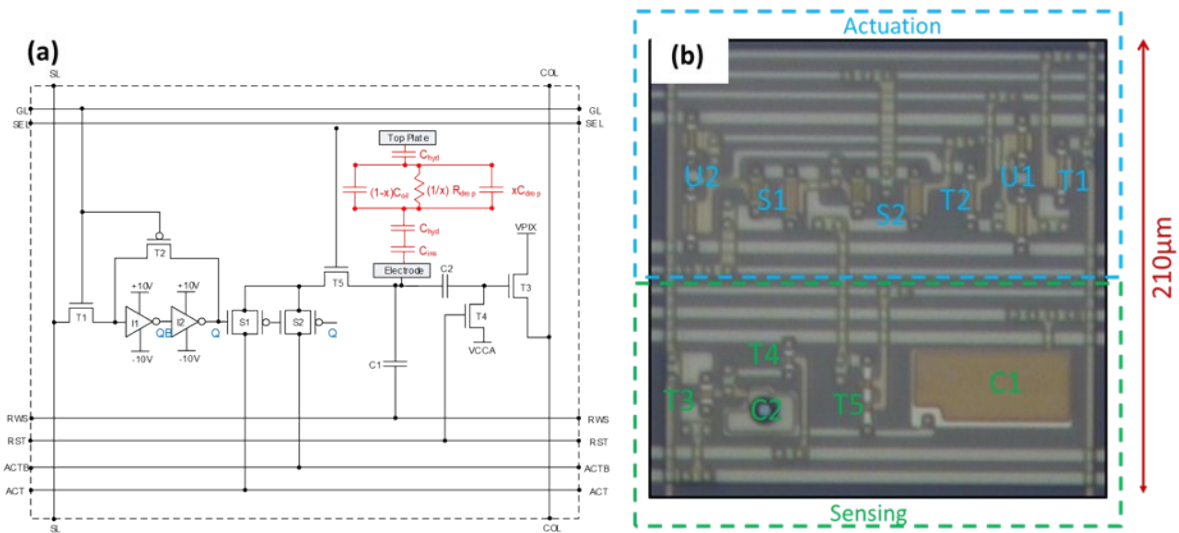


Fig. S1.1. (a) Schematic of the array element circuit. Row and column lines are shown passing through the element in the horizontal and vertical directions respectively. Other input signals and supplies are global. Components in red show a simplified model of the electrical load between the array element electrode and the common electrode of the top plate,  $C_i$  and  $C_h$  representing the capacitances of the insulator layer and hydrophobic coatings, any liquid droplet present is modelled as a capacitor  $C_D$  in parallel with resistor  $R_D$ ; (b) Micrograph of the array element circuit with components labelled; (c) Exemplary timing chart to illustrate normal mode operation; (d) Exemplary timing chart to illustrate self-test mode of operation

## S2: Droplet manipulation algorithms

This section describes how droplet manipulation algorithms are optimised to reduce / remove second order parasitic effects. The various techniques described illustrate the power of the TFT based approach to DMF; the ability to have many and small diameter electrodes facilitates modes of operation where the droplet covers many electrodes simultaneously, enabling the precise control of droplets. Similarly, the high sensitivity of the TFT-based capacitance sensor can be used to detect unwanted parasitic effects such as bubbles of gas or oil.

### Droplet operations with edge-based actuation

In typical TFT-DMF operation, the manipulated droplets have a footprint that covers multiple array elements, typically 3x3 or more. Since the electro-wetting effect occurs at the contact line, according to first order theory, it is unimportant whether array elements internal to the droplet (i.e. completely covered by liquid) are actuated or not. However, in the case where the top plate hydrophobic coating is well insulating (as it is found to be in our devices), the proportion of the droplet footprint does have an effect on the internal droplet potential, as shown in Figure S2.1. By applying actuation only at the contact line, the droplet potential is maintained close to that of the top plate electrode. This minimises the potential dropped across the top substrate hydrophobic coating, which is found to be advantageous for preventing bubble formation at high temperatures.

The droplet potential  $V_{DROP}$  in a droplet whose footprint covers  $n$  electrodes is given as a function of the potentials and strength of capacitive coupling to the electrodes in its vicinity and is given by:

$$V_{DROP} = V_I + \frac{nC_{Cy2}V_{TOP} + \sum_i (C_{bi}V_{Bi})}{C_{TOTAL}}$$

Where  $C_{Cy2}$  is the capacitance between the droplet and the top plate electrode associated with the top plate Cytop coating,  $C_{bi}$  is the capacitance from the droplet to array element electrode  $i$ ,  $V_{TOP}$  is the instantaneous top plate potential,  $V_{Bi}$  is the potential of array element electrode  $i$ ,  $C_{TOTAL}$  is the total capacitance, and  $V_I$  is a DC offset potential, whose initial value is determined by the potential of the liquid upon input. Prior to entry into the cartridge, the droplet material may be pre-charged, e.g. if it is dispensed from a charged plastic pipette.  $V_I = 0$  ( $V_{DROP} = V_{TOP}$ ) can be ensured by designing the device such that hydrophobic coating upon the top plate is removed (photo patterned) in an annulus of approximately 100 $\mu$ m width around the input port. The (hydrophilic) annulus created is found to have no deleterious impact upon effect fluid loading but has the benefit of ensuring the liquid directly contacts the top plate electrode upon fluid input and discharges to the top plate potential.

In the device of our design (coating thicknesses and permittivities)  $C_{Cy2} \sim 3C_b$ . Consequently, if all of the array elements beneath a droplet are actuated, the potential dropped across the top plate Cytop coating is  $V_{Cy2} = 0.25 V_{EW}$ . However, if edge actuation is employed such that only 20% of the footprint of the droplet is actuated  $V_{Cy2} = 0.025 V_{EW}$ . The main benefit of using edge actuation is that by reducing the electric field through the top plate hydrophobic coating, parasitic bubble formation at high temperatures is eliminated. Whilst the exact mechanism for bubble formation is not clear, a clear correlation is observed with the proportion of array elements actuated and the electro-wetting voltage applied. It is found that by appropriate use of edge actuation, the generation of bubbles can be eliminated. A second benefit of edge-based actuation, is that a larger majority of the applied electro-wetting voltage is dropped across the coating layers of the TFT substrate, where it is desirable. This facilitates electro-wetting operation at lower voltages (of up to 25%).

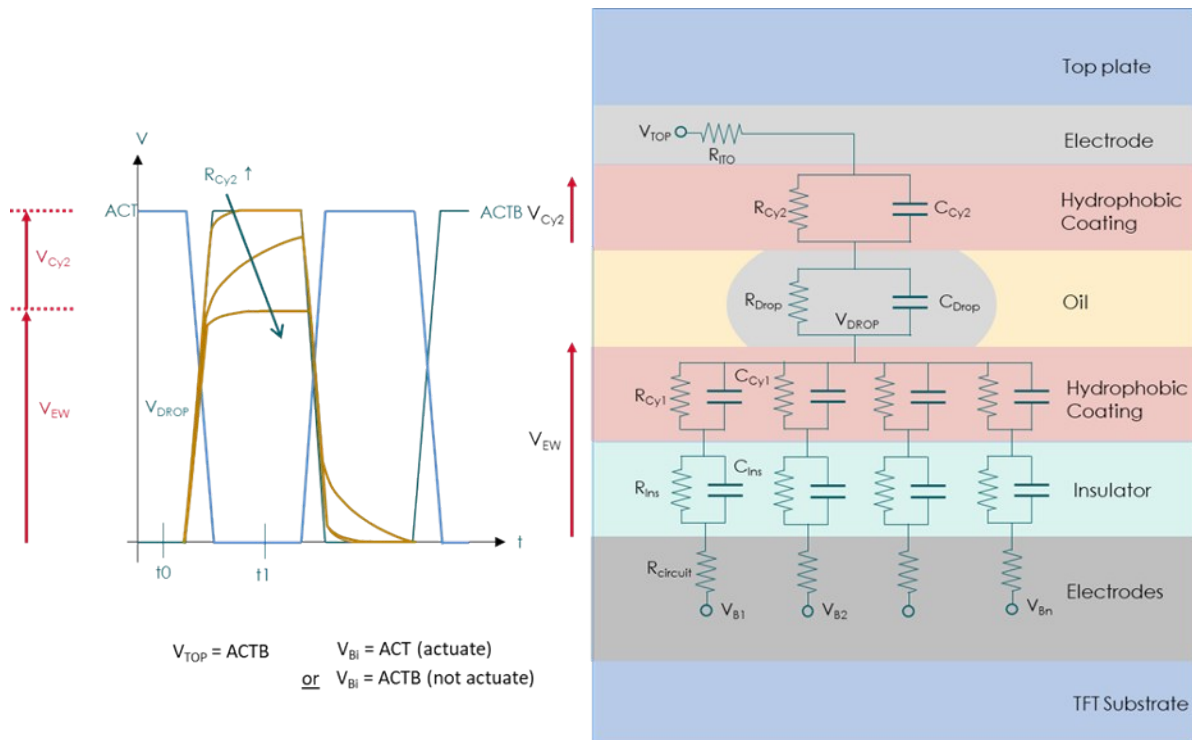


Fig. S2.1 Model for internal droplet potential, showing (left) the time variation of the droplet potential as a function of the time varying signals applied to the electrodes, and (right) an electrical model of the EWOD cell.

### Droplet operation for oil removal from droplet interior

Whilst operation of DMF devices with a filler fluid (oil) has many benefits, it is well known that this can result in thin films of oil being present between the droplet and the coated surfaces [2]. Whilst the oil film, it's potential to collapse when actuation is applied can result in small pockets of oil being trapped within the droplet perimeter. Oil may also become trapped within a droplet upon performing a merge operation. Whilst such trapped oil pockets are not catastrophic for operation, they are nevertheless unfavourable, since expansion of the droplet perimeter can result in incorrect measurement and metering of droplet volumes by the TFT sensor, thus compromising the 2% accuracy and precision in size measurement that the electronics is otherwise able to achieve [3]. Accordingly, there is motivation to employ a droplet operation to remove trapped oil immediately after merging droplets and/or immediately before performing critical (metered) steps, e.g. droplet splitting. Figure S2.2 illustrates this operation, which uses an inverted electrowetting pattern to transport a pocket of trapped oil which traverses a path defined by the unactuated electrodes from the interior of the droplet to the perimeter. The oil removal operation may also be performed based upon TFT capacitance sensor detection of a trapped oil pocket, or using sensor feedback to manipulate the pocket to the droplet perimeter.

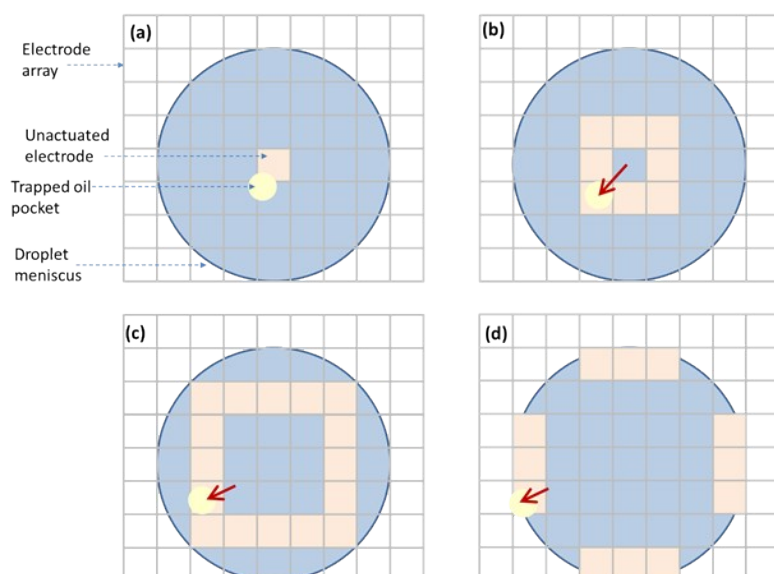


Fig. S2.2 Exemplary droplet operation for removal of trapped oil (shown as a yellow circle) from a droplet interior, showing successive actuation patterns (a) to (d). The unactuated electrodes are shown shaded orange and attract the oil pocket by reverse electrowetting. Consequently any oil pocket present within the droplet is swept to the perimeter before passing out through the meniscus

### Droplet operation for avoidance of bead aggregation

A similar droplet operation to that shown in Figure S2.2 is found to be effective in preventing unwanted aggregation of solid particles (e.g. magnetic beads) in droplets that contain these. At AC actuation and because the resistance of liquid material is non-zero, weak dielectrophoretic forces are set up within the droplets which act upon the beads and serve to re-circulate them.

### S3: Microfluidic Cartridge

The EWOD cell is made by separately coating the TFT backplane and an ITO coated top glass (Asahi glass, thickness 0.7mm) with 50nm of fluoropolymer (M-type Cytop, Asahi Glass Corporation) using a proprietary dip coating method. The Cytop is patterned by photolithography in regions where electrical contact is made. Fluid is input / extracted *via* holes in the top plate, created by drilling prior to Cytop coating. The TFT backplane and top plate are sealed together and spaced apart from each other by a UV-cured adhesive layer deposited around the perimeter of the top glass and into which acrylic spacer beads are embedded. The cell gap spacing in the plane of the liquid is that of the bead diameter, 238 $\mu$ m with a measured 1-sigma variation of typically  $\pm 10\mu$ m or better achieved within a device and device-to-device, as measured by IR interferometry. The TFT backplane extends beyond the top plate in the region of the electrical connector. Electrical connection from the TFT backplane to the top plate is made with silver loaded epoxy. This part of the device (the microfluidic module) was manufactured by Sharp Corporation. The module was further encased within a custom designed black plastic housing (Protolabs) with fluid input and extract ports designed to align with the holes in the top plate, and finally a custom designed PCB interface connector is bonded to the connection terminals of the glass to realise the fully assembled microfluidic cartridge.

### S4: Control Instrumentation

The microfluidic cartridge is loaded into a custom designed and built instrument. The key components of the instrument are as follows:

*Control electronics* was implemented with custom designed PCBs. The voltages and timing signals required to drive the microfluidic cartridge are generated by an FPGA hosting custom designed VHDL firmware. A sensor circuit measures and digitises the capacitance sensor output. Additional PCBs control the magnetic and thermal systems. The control electronics interfaces by USB2 to a PC integrated within the instrument.

*Control software* is coded in C# in the Windows.Net framework. The low-level modules perform the functions of processing sensor data to determine the size and positions of droplets and define and generate actuation data then communicated to the firmware. Mid-level functions define droplet operations as unitary sequences of actuation data, parameterised by variables such as droplet size, operation execution speed, etc. The droplet operations use feedback, such that an  $(N+1)$ th frame of actuation data is generated from analysis of the  $N$ th frame sensor data. Mid-level operations also control the thermal and magnetic control systems and the detection optics. At a high-level, an application specific script, written in a customised version of the Python language, defines a complete protocol to implement the desired assay in droplet format. The script

provides the capability to chain sequences of operations, organise the execution of parallel chains, track droplets, and manage progress and dependencies, for example as droplets are created by splitting, or annihilated by merging. A Graphical User Interface (GUI) provides the user with control and visualisation and includes a simulation mode to support protocol design.

*Droplet manipulation protocols.* The unit droplet manipulation steps (move, merge, mix, split, dispense) were implemented as closed-loop algorithms in the control software. The actuation patterns applied, their timings in relation to the sensor feedback, and the electro-wetting voltage have been carefully designed to minimise second order parasitic effects, including bubble generation at high temperature (due to electric field across the top plate hydrophobic coating), trapped pockets of oil in the droplet interior, and unwanted aggregation of magnetic beads. Details can be found in part S2 of the Supplementary data.

*Magnetic system.* The instrument is arranged to define three zones proximate to the active area (electro-wetting array) of the microfluidic cartridge. The magnetic system enables the implementation of bead-based clean-up steps on device at eight discrete bead wash locations. The magnetic system comprises an array of eight magnets that can be controlled by the software to move away from or in contact to the back face of the TFT glass. The magnets are conically shaped neodymium the geometry simulated by finite element modelling in design (COMSOL) to maximise the magnetic field gradient in the plane of the liquid in the immediate vicinity of the magnet, whilst minimising interaction between adjacent magnets. To this end, adjacent magnets have alternate N and S poles facing the microfluidic cartridge.

*Thermal control system* Two independently controlled thermal zones are defined, for controlling the temperature in the liquid to between 20- and 100-degrees C, implemented with Peltier heater/coolers (TE Technology, part number VT-31-1.0-1.3), thermistors for measurement and feedback (Pt100 RTD type, Labfacility, part number DM-154), a custom designed aluminium heat spreaders and a custom designed PID control loop built-into the firmware. The temperature achieved in the plane of the liquid was verified. The ramp rate of the system is approximately 1°C/s. The temperature achieved in the plane of the liquid was verified using a dummy cartridge comprising 12 miniaturised K-type thermistors mounted in different positions between glass substrates of the same thickness as used in the microfluidic cartridge.

### S5: Illumina Next Generation Sequencing: DNA Library preparation Protocols on aQdrop

There are many commercially available kits designed to prepare DNA samples for Illumina next generation sequencing. In this section we highlight development work carried out to translate Kapa Hyperplus (Roche) kit at low density, Colibri ES (Thermo Fisher) kit at low and high density and NexteraFlex Enrichment kit (Illumina) at high density for the aQdrop platform. During protocol development low density droplet arrangements were used to test that the chemistry performance on chip was comparable to that in tube. When the chemistry performance was confirmed the number of samples processed per chip was increased to reduce the cost per sample of library preparation. In Fig. S5.1, the TFT chip is illustrated as a checker board and droplets in yellow. The large squares are 8 x 8 electrode elements on the TFT. The numbered circles represent the input port (holes in the ITO top-plate) through which the reagents for a particular protocol are loaded. In the low density aQdrop arrangement there are two variable temperature zones and a zone with 3 magnets. The high density aQdrop chip arrangement has two variable temperature zones and 8 magnets. The standard in tube kit protocols were followed except that they were carried out on a reduced scale and bead pellets were washed with PEG-salt wash buffer in place of ethanol/water and a double elution of final library was performed. After libraries were prepared on aQdrop they were sequenced using Illumina sequencers.

#### 1. Kapa Hyperplus (Roche) DNA Library Prep kit for Illumina

The Kapa Hyperplus DNA library preparation kit was miniaturised and automated on aQdrop at low droplet density. Three reactions at 1/50<sup>th</sup> scale (to tube) were performed in parallel, beads were washed with PEG-salt wash buffer in place of ethanol/water and a double elution of final library was performed. Samples were indexed and then 8 separately prepared libraries were pooled for sequencing with the Illumina HiSeq4000.

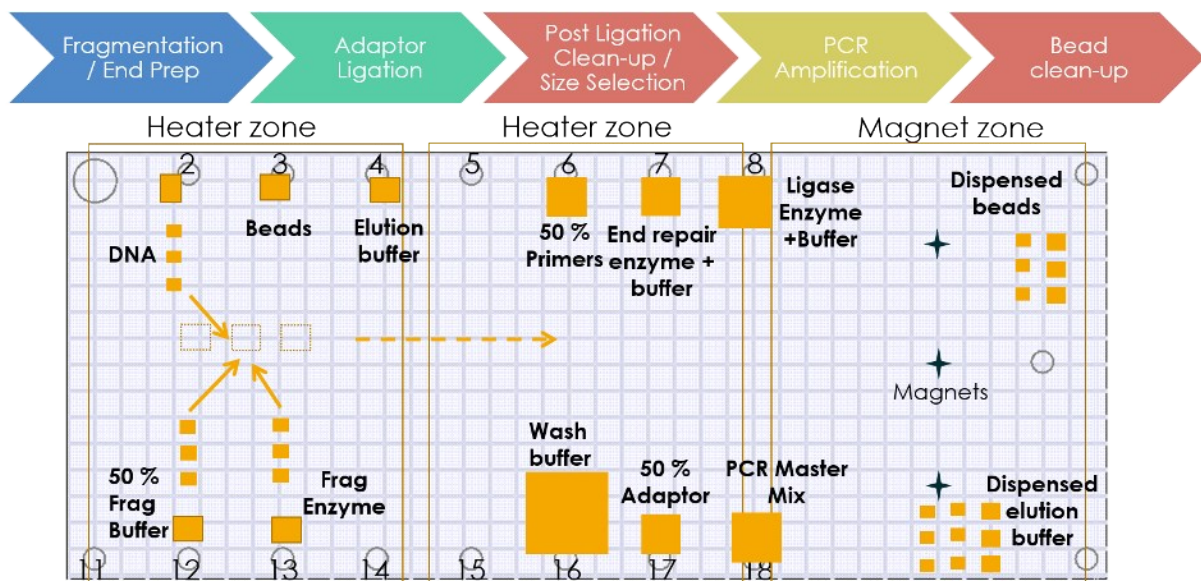


Fig. S5.1 Layout of droplets for aQdrop DNA library preparation (Low Density) with the Kapa Hyperplus kit. The steps carried out in DNA library preparation for NGS are illustrated at the top of the figure.

Sample	% GC	Insert size	% Aligned	% Dups	% Chimera	% Dimer	M Seqs
Index 2 (chip)	42	188	99.2	2.50	4.34	0.08	44.9
Index 3 (chip)	42	174	99.3	1.40	5.05	0.03	44.9
Index 4 (chip)	42	181	99.3	1.40	4.79	0.06	44.9
Index 7 (chip)	42	180	99.3	2.90	5.89	0.03	44.9
Index 9 (chip)	42	184	98.5	2.80	5.19	0.07	44.9
Index 22 (chip)	42	180	98.9	3.20	5.00	0.14	44.9
Index 16 (tube)	42	213	99.0	2.00	4.15	0.03	44.9
Index 27 (tube)	42	239	98.7	2.80	3.69	0.03	44.9

Table. S5.1 Sequencing metrics for 8 pooled libraries prepared using the Kapa Hypercap kit. (Sequenced (HiSeq 4000) by Oxford Genomics Centre, Oxford University). Each DNA library has a different index and data from tube and chip prepared libraries are compared.

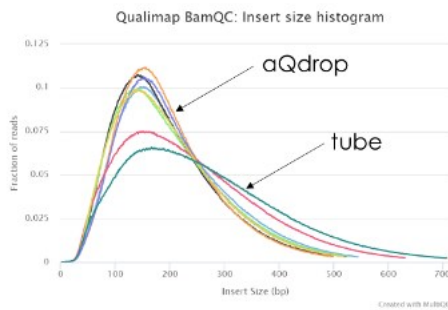


Fig. S5.2 Insert size plotted against the fraction of the total reads

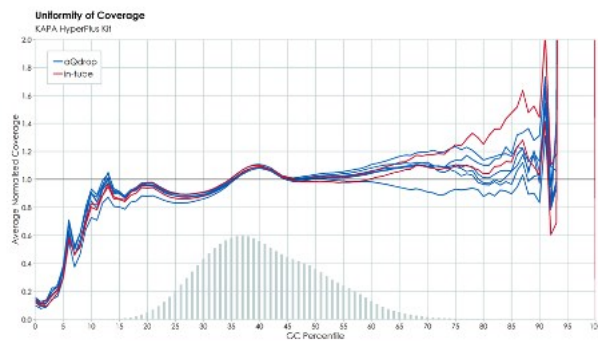


Fig. S5.3 Uniformity of coverage (Libraries sequenced using Illumina HiSeq 4000, Oxford Genomics Centre) – assessing whether the GC content reduces the extent of genome coverage for a particular library. No significant differences between tube and chip were observed.

### 1. Colibri ES (Thermo Fisher Scientific) DNA Library prep. kit for Illumina

Low density protocol development – library preparation with human gDNA

Modifications to standard protocol: the protocol was performed on aQdrop at 1/50th scale, 3 droplets of gDNA were processed in parallel. Beads were washed with PEG-salt wash buffer in place of ethanol/water and a double elution of final library was performed – giving a final 6/50th scale elution volume.

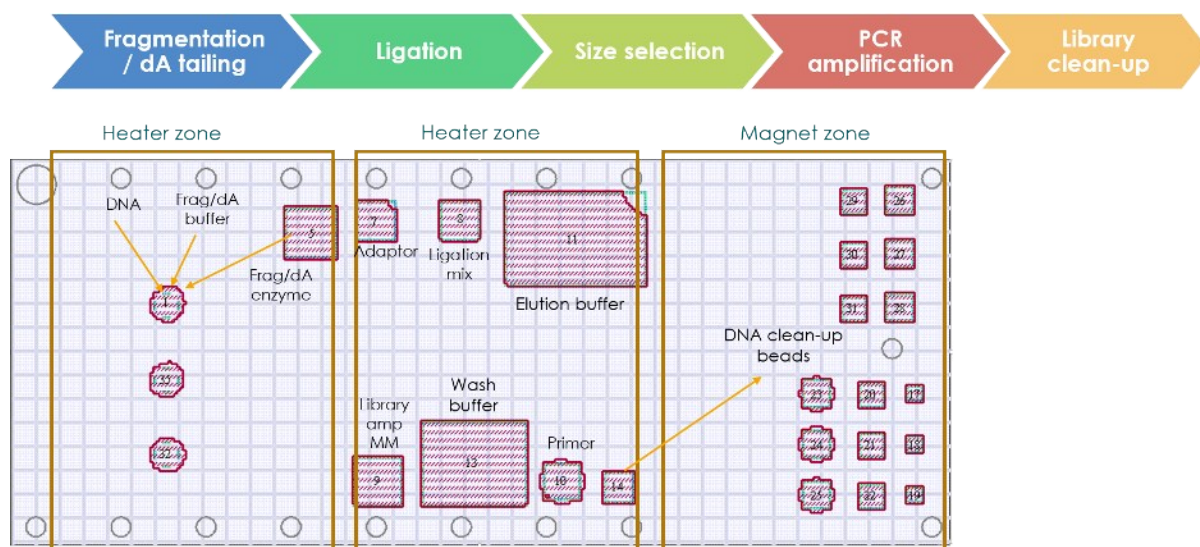


Fig. S5.4 Layout of droplets for aQdrop DNA library preparation (Low Density) from a protocol log file after loading reagents and set-up. The checker board represents the TFT electrode array, the aqueous droplets are shown in red and the actuation patterns in green. The arrows at the top illustrate the library preparation steps being automated on aQdrop.

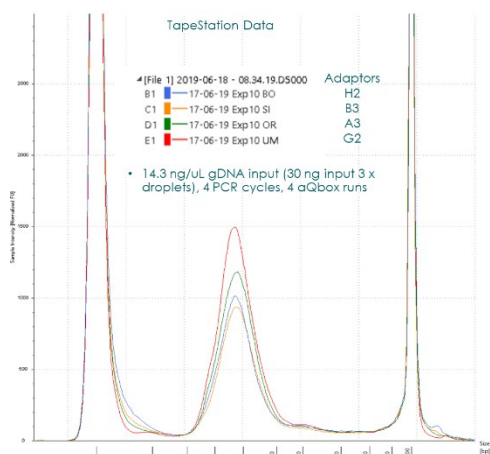


Fig. S5.5 Tapestation analysis of DNA libraries prepared from human genomic DNA on aQdrop (Low Density Protocol)

High density protocol development – demonstration with 3 out of 6 reaction zones operating

The high density protocol is illustrated in Fig. S5.6 for three out of a possible six reaction zones. The DNA samples are loaded at the top of the chip and are then processed in sample specific reaction zones (rectangles shown in black – each with two heaters and a magnet); libraries are collected from the bottom of the reaction zone. In Fig. S5.6 DNA libraries are prepared from bacterial DNA: 3 DNA samples (*E. coli*, *S. aureus*, *P. aeruginosa*) gDNA, 10 ng gDNA per reaction zone, 3 different index adapters. Libraries were analysed on TapeStation see Fig. S5.7. Output concentration varied by DNA input type. *S. aureus*: 2.72 ng/  $\mu\text{L}$ , 6.8 ng; *E. coli*: 3.86 ng/  $\mu\text{L}$ , 9.7 ng; *P. aeruginosa* 1.64 ng/  $\mu\text{L}$ , 4 ng, fragment distribution was consistent, though the average fragment size was larger than expected. Libraries prepared on aQdrop were sequenced on MiSeq (Illumina)



Fig. S5.6 Layout of droplets for aQdrop DNA library preparation (3 out of 6 reaction zones operating)

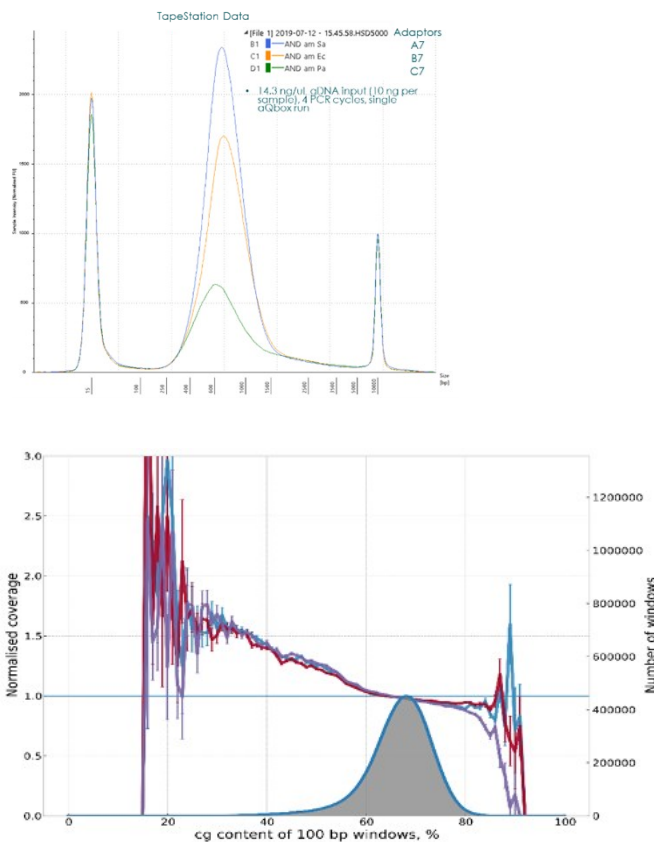


Fig. S5.7 TapeStation analysis of libraries

Fig. S5.8 GC coverage – *Pseudomonas aeruginosa* (MiSeq Illumina)

## 2. Illumina NexteraFlex Enrichment Library Preparation on aQdrop

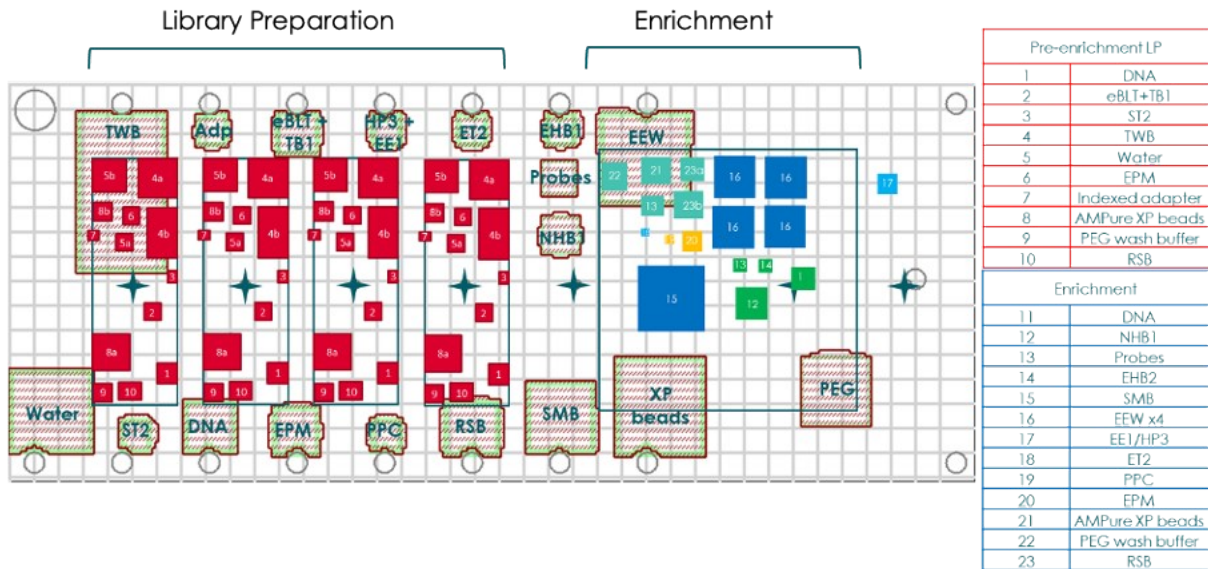


Fig. S5.9 Layout of droplets for aQdrop are taken from a log file just after reagent and sample loading. The reservoirs from which the droplets are dispensed are shown near the input ports and labelled according to the various kit reagents. The sensor images of the droplets are shown with wavy red lines and the actuation patterns holding the droplets in place in green. The droplet arrangement for the DNA library preparation (after droplet dispense, is superimposed in solid red) is repeated in parallel four times and feeds into 1 x hybridisation enrichment (RHS droplets shown in blue, green, yellow and turquoise).

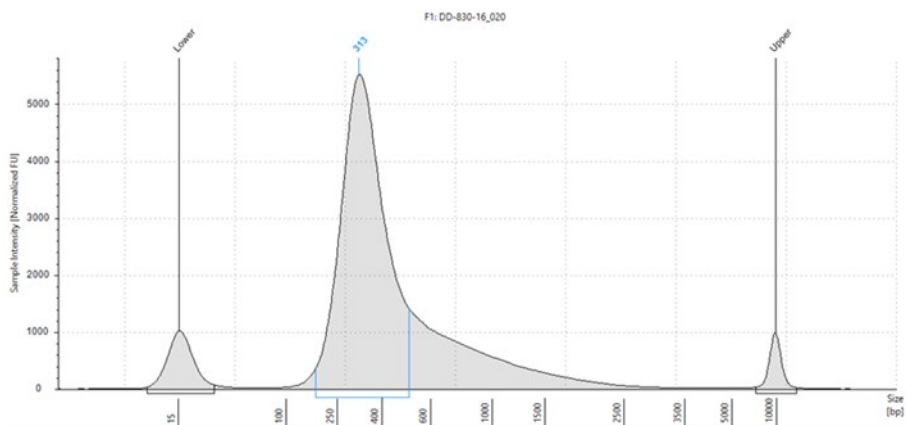


Fig. S5.10 Tapestation analysis from library prep. on aQdrop x 4

Index	Input/ng	Conc Sample Qubit (ng/ $\mu$ L)	Conc sample TS (ng/ $\mu$ L)	Peak frag (bp)	Mean frag (bp)	ng out	Yield (Qubit)
JAB 1-4 E1	15.38	17.16	12.06	313	410	34.32	2.2

Table S5.2 Summary of DNA library characteristics. Pooled sample ready for enrichment protocol

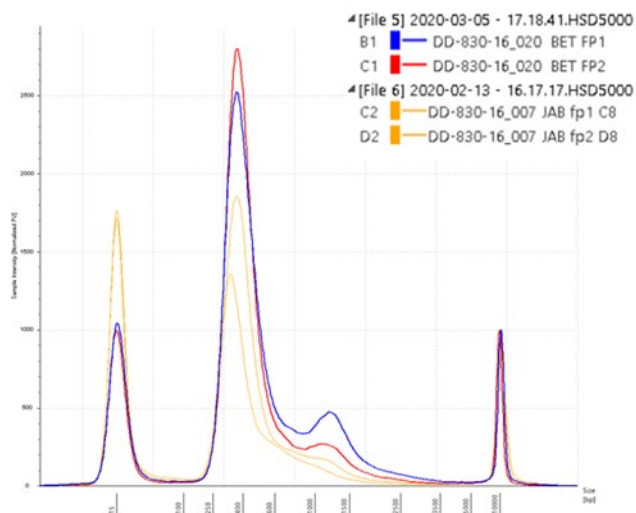


Fig. S5.11 TapeStation analysis of on aQdrop enriched libraries (CEX probes)

Index	Input/ng	Conc Sample Qubit (ng/ $\mu$ L)	Conc sample TS (ng/ $\mu$ L)	Peak frag (bp)	Mean frag (bp)	ng out	Yield (Qubit)
BET 1 A8	99.96	7.76	10.96	359	448	7.76	0.1
BET 2 B8	75.24	4.00	5.22	369	431	8	0.1

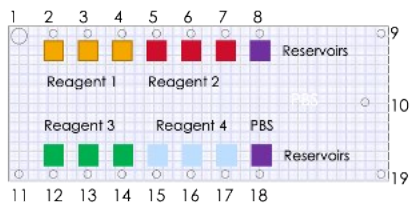
Table S5.3 Summary of DNA enrichment library characteristics.

## S6: Protocol Development on aQdrop for IVD at the Point of Need

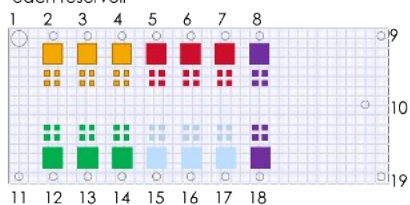
**Reagent Speed and Dispense Tests:** To check compatibility of kit reagents with our aQdrop filler-fluids. Our standard speed and dispense test scripts were run with all reagents. The tests were automated as a Python script to be executed through the software GUI. Details of the methods are illustrated in Fig. S6.1.

### Dispense Test

1. Load samples to generate reservoirs when prompted by script (4 different reagents (in triplicate) and PBS (duplicate)).



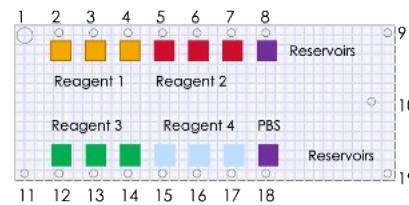
2. Set voltage to required value. Four droplets dispensed from each reservoir



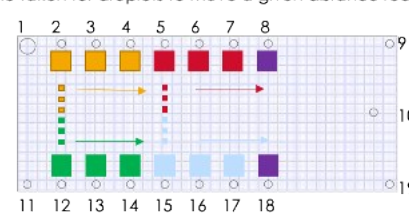
3. Droplet sizes recorded. Droplets returned to reservoirs and dispense repeated (total of 8 droplets dispensed per reservoir). Repeat steps 2 and 3 for voltages = 16, 18, 20 V.

### Speed Test

1. After dispense test has completed dispense 3 droplets from 4 chosen reservoirs



2. Time taken for droplets to move a given distance recorded



3. Speed test repeated at voltages 12, 14, 16, 18 and 20 V  
4. Repeat speed test for other reservoirs

Fig. S6.1 Details of aQdrop Speed and Dispense Test methodology.

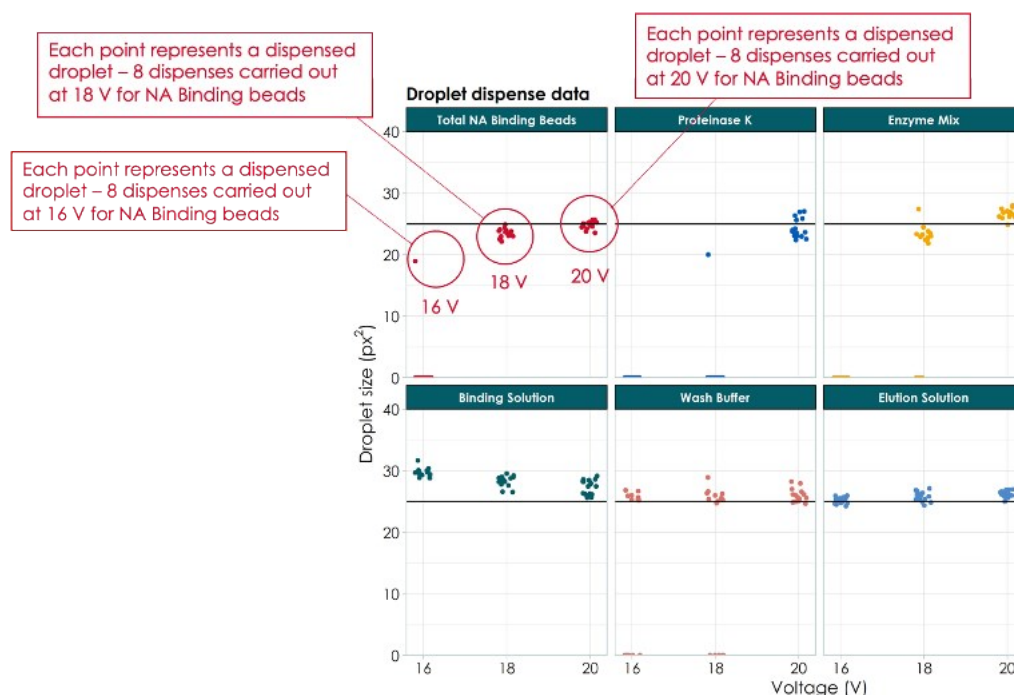


Fig. S6.2 Dispense test results for reagents from the Thermo Fisher MagMax Viral/Pathogen Nucleic Isolation Kit: actuation type = full actuation, feedback type = closed loop, filler-fluid = Genomics, room temperature, set droplet size = 5x5 elements, voltage = 16, 18, 20V. Horizontal black line corresponds to the droplet size set in the script (25 elements in this example); deviation between the set value and the measured droplet size relates to non-optimised dispense parameters

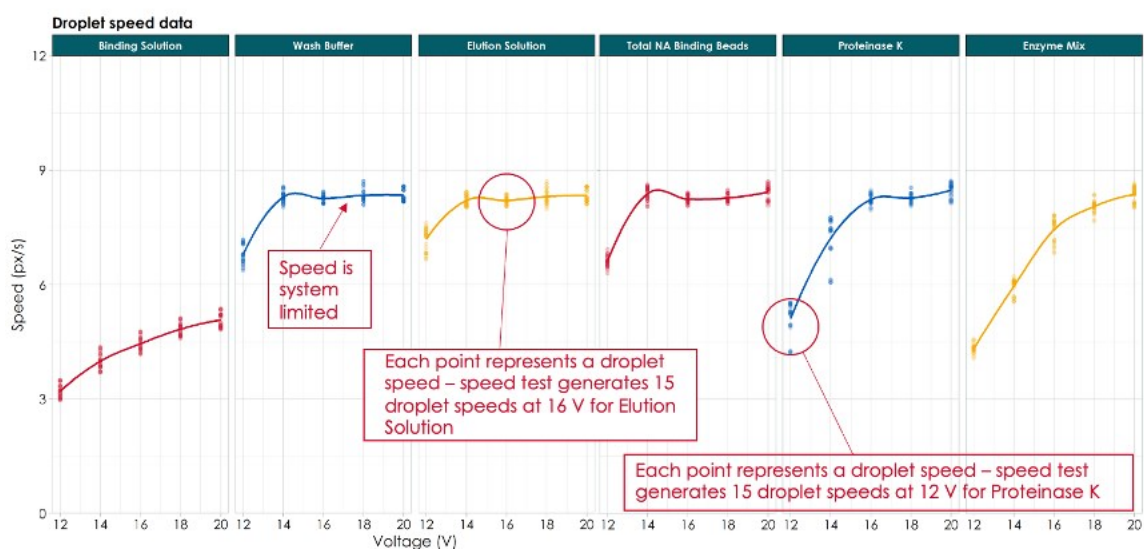


Fig. S6.3 Speed test results for reagents from the Thermo Fisher MagMax Viral/Pathogen Nucleic Isolation Kit: reagents loaded in triplicate (see Fig. S6.1), four reservoirs chosen for the speed test at a given voltage, each reservoir used to dispense 3 droplets, those 3 droplets moved 5 x across cartridge to generate 5 droplet speeds per droplet (only considering movement to the right), voltage incremented by 2 V from 12 to 20 V and the speed test repeated for each voltage

As with all our on aQdrop experiments the script informs the user when and what to load into the aQdrop cartridge. In the set-up stage, reagents were input into the cartridge by pipette. Electro-wetting control was used to capture the input liquid onto designated array elements in proximity to the port to form a reservoir, and feedback from the sensor was used to verify that the correct volumes had been input into each port. Droplets of the various reagents were then dispensed from reservoirs and moved with a range of voltages to assess (a) voltage vs droplet size (Fig. S6.2) and (b) voltage vs droplet speed (Fig. S6.3). All reagents from the various kits described in the methods section of the paper were found to electrowet and move well with our genomics filler-fluid (dodecamethyl pentasiloxane containing Brij52 (0.08 % w/w)) at 20 V.

**Protocol steps:** The various protocol steps were performed independently and the outcome of each step confirmed by analysis with standard laboratory methods. Where appropriate the protocol steps were also carried out in-tube for comparison. Details of the nucleic acid extraction step are detailed in the accompanying paper.

**RT-PCR Light Cycler 96:** RT-PCR experiments with Primer Design, Thermo Fisher and Kapa enzyme systems were assessed under standard conditions in Light Cycler experiments. The Kapa enzyme was an interesting alternative having a lower temperature RT step (42 °C rather than 50/55 °C) and RT and PCR enzymes packaged separately for optimisation. The differences in turn-on times for samples templated with DNA (Primer Design positive DNA control) and RNA (AcroMetrix, Thermo Fisher) of the same copy number are reported in Table S6.1. The Thermo Fisher RT-PCR enzyme system was found to perform best, and the Kapa system worst. The performance of the Kapa enzyme system was improved by doubling the amount of reverse transcription enzyme in the RT-PCR protocol, suggesting that performance of the other enzyme systems might be improved by modifying the ratios of reverse transcription to PCR enzymes. The difference in turn-on for DNA and RNA templated reactions using the Thermo Fisher enzyme system was 2.5 cycles. An estimate can be made that there is  $2^{2.5}$  (i.e. 5.7) times more DNA in the reaction mixture directly templated with DNA than that templated with RNA that is converted to cDNA during the reverse transcription step. This suggests that the yield for the reverse transcription step is about 20 % under these conditions. The relatively low yield for reverse transcription means that where there are only a few copies of viral RNA or when carrying out RT-PCR on aQdrop (where the volume is small) very few or no copies of cDNA will be made during reverse transcription thus generating a false negative. We believe that optimisation of reverse transcription on aQdrop through a two-step RT-PCR process will give significantly better results, and since the whole protocol is automated no increase in hands-on-time.

Enzyme System	Reverse transcription temperature (°C)	Nucleic acid concentration (copies / $\mu$ L)	$\Delta C_q$ (Cycles)
Primer Design	55	10	3.8
Thermo Fisher TaqMan Fast Virus 1-Step Master Mix (4444432, Applied Biosystems, Thermo Fisher)	50	20	2.5
Kapa Probe Fast Universal 1-step qRT-PCR Master Mix (KK4752, Merck/Sigma Aldrich)	42	20	5.12
Kapa (2 x RT enzyme concentration)	42	20	3.79

Table S6.1 Comparison of RT-PCR performance for Light Cycler 96 standard reactions templated with DNA (Primer Design Positive Control supplied with kit) and RNA (Coronavirus RNA, AcroMetrix, Thermo Fisher).  $\Delta C_q$  (Cycles) refers to the difference in turn-on time observed for equivalent RT-PCR tests templated with the same copy number DNA or RNA.

To obtain a better understanding of RT yield, a range of Coronavirus RNA concentrations should be assessed in the same way that the various DNA template concentrations were used to generate a standard curve for the DNA templated qPCR process.

*RT-PCR on aQdrop:* Initial incompatibility between the Primer Design enzyme system and the aQdrop platform was overcome by using MagMax elution buffer in the RT-PCR reaction mixture rather than water. Under these conditions RT-PCR was possible in droplets on aQdrop in the Genomics filler-fluid, whereas in the absence of the Elution Buffer, droplets were found not only to move more slowly as they were mixed during reverse transcription and to be stuck to the aQdrop device surface after the PCR hot-start, but to show no DNA amplification during PCR; no change in fluorescence of the droplets during thermal cycling was observed and analysis by electrophoresis (Tapestation) of droplets after RT-PCR showed none of the expected amplicon formation.

*qPCR Light Cycler 96:* The standard curve illustrated in Fig. S6.4 was plotted from Light Cycler generated PCR data for comparison with the aQdrop standard curve (see results section of paper).

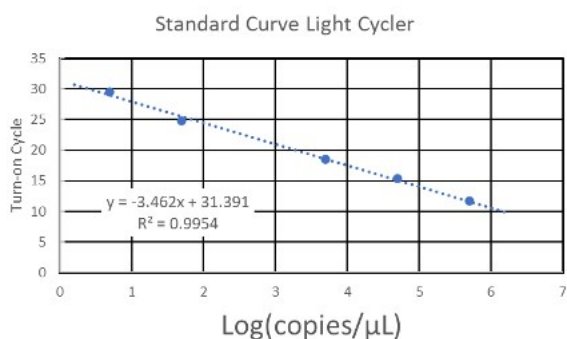


Fig. S6.4 Standard curve for qPCR in the Light Cycler 96 for comparison to the aQdrop data.

### Droplet Digital PCR on aQdrop:

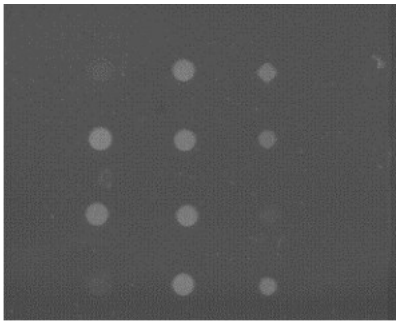


Fig. S6.5 Fluorescence image of 4 x 3 array of droplets after thermal cycling on aQdrop originally containing 1 or 0 copies of DNA. For a droplet size of 0.3  $\mu$ L single copy turn-on is clearly discernible.

### Combined Protocol Steps on aQdrop:

#### Nucleic Acid Extraction, DNase treatment and RT-PCR with two targets –Primer Design enzyme system

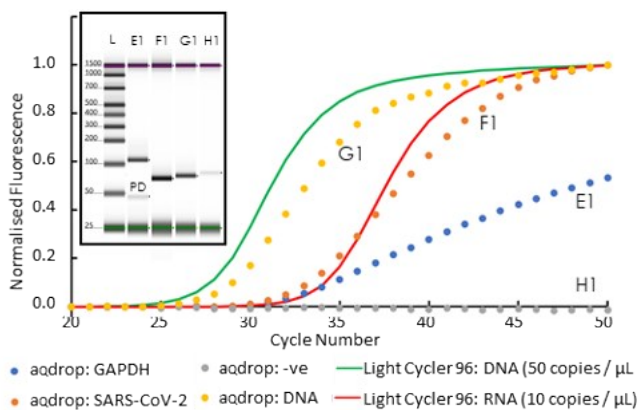


Fig. S6.6 RT-PCR amplification curves derived from fluorescence images taken by the aQdrop system for a qualitative SARS-CoV-2 test and proof of concept host response assessment (GAPDH). Inset: electrophoresis data for droplets extracted from the aQdrop device (D1000 Tapes, Agilent TapeStation): L – Ladder, E1 – GAPDH target (PD refers to signal corresponding to primer dimers), F1 – SARS-CoV-2 target, G1 – DNA positive control, H1 – negative control.

The data points represent the average cycle-by-cycle fluorescence output from pairs of droplets on aQdrop. In this example, RT-PCR output from positive (DNA) and negative controls are compared with the output from nucleic acid sample derived from saliva spiked with Coronavirus RNA assessed for SARS-CoV-2 RNA (orange), and human GAPDH RNA (blue). The solid lines are Light Cycler 96 derived amplification curves for SARS-CoV-2 DNA and RNA positive controls and are included for comparison. As was expected, turn-on was observed for the nucleic acid sample in both the Coronavirus (SARS-CoV-2, orange dots) and human GAPDH assays (blue dots) and the DNA positive control (yellow dots), whereas no turn-on was observed for the negative control (grey dots). These results confirmed that the sample contained Coronavirus RNA, that PCR amplification on aQdrop had similar performance to PCR in a standard laboratory thermal cycler (from the DNA positive control).

*Estimating Coronavirus copy number:* With no RNA positive control on aQdrop the DNA positive control was used alongside the difference in turn-on observed in the Light Cycler 96 for samples having the same copy DNA and RNA copy numbers. The number of copies of Coronavirus RNA in the original sample was calculated to be 160. This is only 25 % of the total number of copies of RNA originally added to the saliva sample.

*GAPDH amplification curve:* The GAPDH assay fluorescence output on aQdrop showed an almost linear increase in fluorescence with cycle number, suggesting that the amplification is inhibited on aQdrop. The turn on is similar to that for Coronavirus RNA. Electrophoresis data (faint band labelled PD lane E1, inset Fig. S6.6) showed the formation of primer dimers indicative of inefficient PCR.

*DNase treatment:* To assess the performance of DNase on aQdrop, electrophoresis analysis of RT-PCR cycled droplets was carried out under conditions for analysing genomic DNA (genomic Tape and Tapestation). No detectable signal corresponding to genomic DNA was observed whereas after spiking human genomic DNA into these samples and reanalysing them for genomic DNA, signals corresponding to gDNA could be seen (Fig. S6.7).

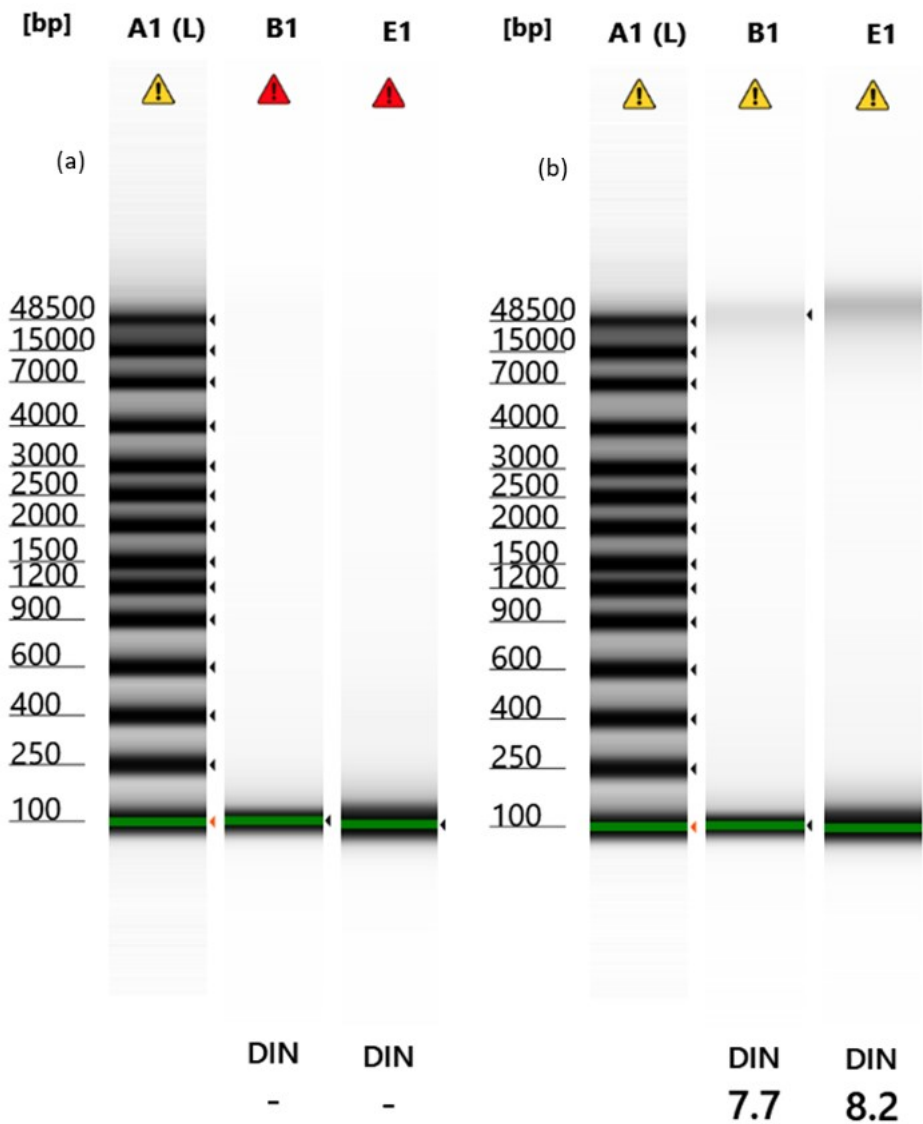


Fig. S6.7 Tapestation (genomic Tape lanes B1 and E1) analysis of droplets from nucleic acid extraction, DNase treatment and RT-PCR amplification; B1 SARS-CoV-2 target, E1 GAPDH target. (a) at the end of the aQdrop protocol (b) sample (a) spiked with human genomic DNA. No evidence for gDNA was observed in the sample after RT-PCR suggesting that DNase treatment had successfully degraded all dsDNA during the aQdrop protocol.

*DNase – Amplicon experiments*

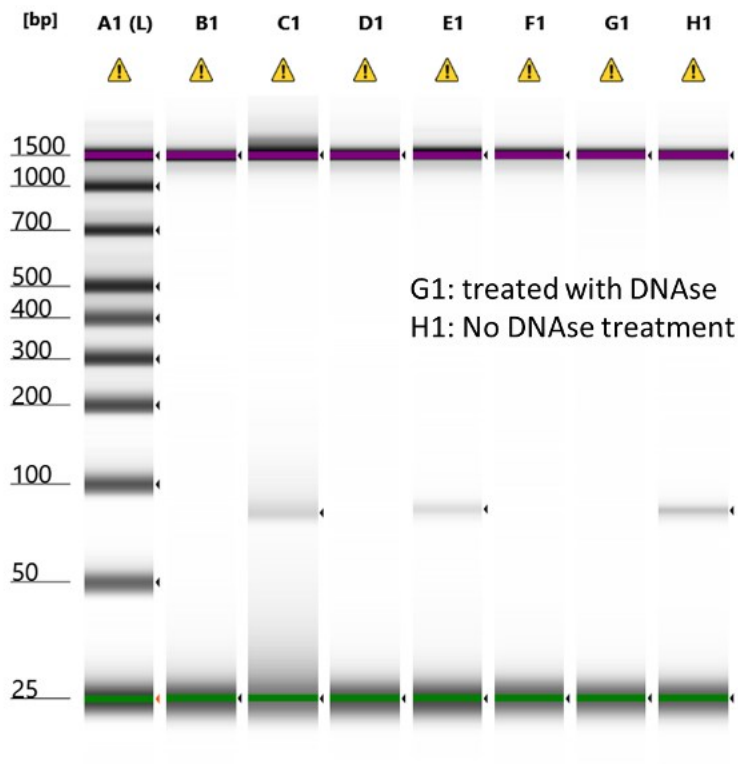


Fig. S6.8 DNase treatment of amplicon dsDNA (positive control from Primer Design 2019 n-CoV genesig Standard kit - expected size about 80 base pairs). Tapestation analysis (D1000 Tape) of dsDNA treated with DNase according to the EZDNase kit instructions lane G1; No DNase treatment Lane H1.

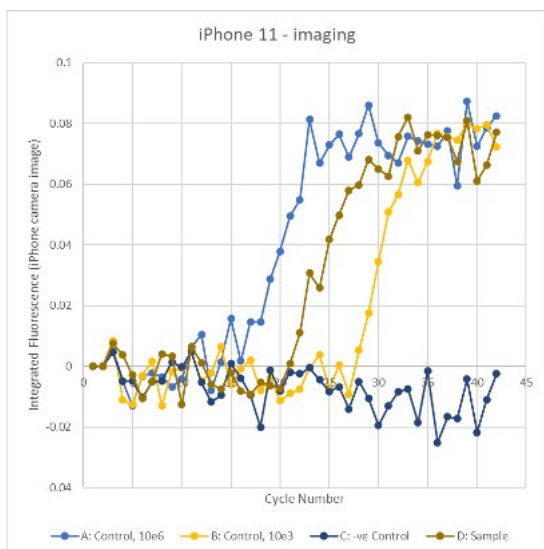


Fig. S6.9 Amplification curves from PCR with Primer Design nCoV DNA positive control:  $1 \times 10^6$  copies / 20  $\mu$ L, 1000 copies / 20  $\mu$ L,  $5 \times 10^4$  copies / 20  $\mu$ L

## **S7: Description of Supporting Videos**

### **Videos**

S1. Next Generation Sequencing Library Preparation: example protocol with colored dyes illustrating 8 parallel independent streams (speed x 20)

S2. aQdrop Workflow Demo

S3. RT-PCR Cycle-by-Cycle Fluorescence Imaging - Time Lapse Video

S4. TFT Chip Sensor Output (speed x 64) - Full sample-to-answer SARS-Cov-2 protocol: nucleic acid extractions, dsDNA degradation and RT-qPCR

### **S8: References**

1. Kumari, V. Bahadur, S.V. Garimella (2008). Electrical actuation of electrically conducting and insulating droplets using ac and dc voltages. *J. Micromech. Microeng.*, 18, 105015
2. Adrian Staicu and Frieder Mugele (2006). Electrowetting-Induced Oil Film Entrapment and Instability, *Phys. Rev. Lett.* 97, 167801
3. Sumit Kalsi, Martha Valiadi, Maria-Nefeli Tsaloglou, Lesley Parry-Jones, Adrian Jacobs, Rob Watson, Carrie Turner, Robert Amos, Ben Hadwen, Jonathan Buse, Chris Brown, Mark Sutton and Hywel Morgan, Rapid and sensitive detection of antibiotic resistance on a programmable digital microfluidic platform, *Lab Chip*, 2015,15, 3065-3075